









Diagnostic Performance of Simulated Abbreviated MRI for Early-Stage Hepatocellular Carcinoma Screening: A Comparison to Conventional Dynamic Contrast-Enhanced MRI

초기 간암 선별 검사로서 단축 자기공명영상 검사의 진단능: 고식적 역동학적 자기공명영상검사와의 비교

Eun Sol Lim, MD¹ , Sung Mo Kim, MD¹ , Sang Soo Shin, MD¹ ,
Suk Hee Heo, MD² , Jong Eun Lee, MD¹ , Yong Yeon Jeong, MD^{2*} 

¹Department of Radiology, Chonnam National University Hospital, Gwangju, Korea

²Department of Radiology, Chonnam National University, Hwasun Hospital, Hwasun, Korea

Purpose To compare the per-patient diagnostic performance of simulated abbreviated MRI (AMRI) to that of conventional MRI (CMRI) with full-sequence dynamic gadoteric acid (GA) enhancement for early-stage hepatocellular carcinoma (HCC) screening in high-risk patients.

Materials and Methods A total of 201 consecutive patients at high-risk for HCC, who underwent 3T liver MRI, were included in this retrospective study. The AMRI protocol comprised T2-weighted imaging, hepatobiliary phase imaging after GA injection, and diffusion-weighted imaging. For each patient, two AMRI and CMRI image sets were independently reviewed by two radiologists. Inter-reader agreement was assessed using Cohen's kappa value. A composite reference standard was used to determine the diagnostic performance of each image set for each reader.

Results A total of 93 HCCs were detected in 79 patients. The inter-reader agreement was almost perfect for both image sets ($\kappa = 0.839, 0.948$). In AMRI, the per-patient sensitivity and negative predictive values (NPV) were 94.9% and 96.4%, respectively. In CMRI, the per-patient sensitivity and NPV were 96.2% and 97.5%, respectively.

Conclusion AMRI, using only three sequences, had a comparable diagnostic performance to CMRI in screening early-stage HCC. AMRI could be an alternative HCC screening tool for high-risk HCC patients.

Index terms Hepatocellular Carcinoma; Liver; Magnetic Resonance Imaging

Received October 5, 2020
Revised October 27, 2020
Accepted October 30, 2020

***Corresponding author**

Yong Yeon Jeong, MD
Department of Radiology,
Chonnam National University,
Hwasun Hospital,
322 Seoyang-ro, Hwasun-eup,
Hwasun 58128, Korea.







Tel 82-61-371-7106

Fax 82-61-371-7133

E-mail yjeong@jnu.ac.kr

This is an Open Access article distributed under the terms of the Creative Commons Attribution Non-Commercial License (<https://creativecommons.org/licenses/by-nc/4.0>) which permits unrestricted non-commercial use, distribution, and reproduction in any medium, provided the original work is properly cited.

ORCID iDs

Eun Sol Lim 
<https://orcid.org/0000-0003-1538-111X>
Sung Mo Kim 
<https://orcid.org/0000-0001-5567-3972>
Sang Soo Shin 
<https://orcid.org/0000-0002-5752-7431>
Suk Hee Heo 
<https://orcid.org/0000-0002-9497-8952>
Jong Eun Lee 
<https://orcid.org/0000-0002-8754-6801>
Yong Yeon Jeong 
<https://orcid.org/0000-0001-6096-3130>

INTRODUCTION

Hepatocellular carcinoma (HCC) was predicted to be the sixth most commonly diagnosed cancer and the fourth leading cause of cancer death worldwide in 2018 (1). A previous study has shown that screening for HCC using ultrasound improved patient survival by permitting the early detection of HCC (2). The American Association for the Study of Liver Diseases and many international organizations recommend semi-annual HCC surveillance using ultrasound for high-risk patients to detect HCC at an early stage (3-5). Despite its low cost and high availability, the per-patient sensitivity of ultrasound for the detection of small and early HCCs is not reliable, as low as 60%–63% according to previous meta-analyses (6). Tzartzeva et al. (7) reported that US detected any stage HCC with 84% sensitivity, but early stage HCC with only 47% sensitivity.

Dynamic contrast-enhanced MRI is proposed for HCC surveillance because of its high diagnostic accuracy for the detection of early stage HCC (< 3 cm) (8, 9). However, the high cost of individual dynamic contrast-enhanced MRI as well as relatively long examination times is an obstacle for the detection of HCC (10). Abbreviated MRI (AMRI), using only a few sequences of MRI, could be an alternative method for HCC screening if the AMRI could provide adequate diagnostic performance for HCC screening. There have been several studies with variable protocols for HCC detection and have shown its usefulness for HCC screening in the high-risk group of HCC (11-17). The AMRI protocols include T2-weighted imaging (T2WI) as a standard and can be divided into two protocols, including hepatobiliary phase (HBP) imaging after gadoteric acid (GA) enhancement.

Treatment options and clinical outcomes in patients with HCC depend primarily on the stage of the tumor at the time of diagnosis (18-20). In that sense, the detection of early stage HCC is more meaningful in screening high-risk populations for curative treatment and prolonged survival. Most AMRI studies have analyzed stage HCCs, including advanced stage and early stage, in the detection of HCCs. Only two studies have evaluated the role of AMRI in the detection of early stage HCC (14, 15). Two studies reported the diagnostic performance of AMRI combined with multiphase CT (14) or an unenhanced AMRI protocol for detecting HCC (15). Park et al. (14) reported that AMRI comprising HBP, T2WI, and diffusion-weighted imaging (DWI) plus multiphase CT showed comparable accuracy (91.2% vs. 87.6%), positive predictive value (PPV) (94.1% vs. 93.5%), and sensitivity (96.4% vs. 92.9%) to full-sequence gadoteric acid-enhanced MRI using Liver Imaging Reporting and Data System (LI-RADS)-4/5 criteria in the HCC screening cohort. Another study (15) showed that the sensitivity of an unenhanced AMRI for detecting HCC of readers 1 and 2 was 88.0% and 86.2%, respectively.

The purpose of this study was to retrospectively evaluate the per-patient diagnostic performance of a simulated AMRI protocol consisting of T2WI, GA-enhanced HBP imaging, and DWI compared to conventional MRI (CMRI) for early stage HCC screening in high-risk patients.

MATERIALS AND METHODS

This single-center retrospective study was approved by our Institutional Review Board (IRB No. CNUHH-2020-121), and informed consent was waived. Patients who underwent GA-en-

hanced liver MRI at the hospital over a 2-year period from January 2017 to December 2018 for HCC screening/surveillance or diagnosis were included in this study ($n = 330$). To avoid duplication, only the first examination was included in each patient. The inclusion criteria included high-risk factors for HCC, such as liver cirrhosis. The exclusion criteria included a history of known HCC with previous treatment ($n = 34$), no follow-up examination ($n = 59$), and other malignancies with metastasis ($n = 3$). To compare the diagnostic performance of HCC screening and surveillance in the early stage, patients with advanced HCCs with $> four$ HCCs ($n = 14$), HCCs larger than 3 cm ($n = 18$), or diffuse infiltrative HCCs ($n = 4$) were excluded. Finally, 201 patients were included in the study (Fig. 1).

Patient demographics and clinical characteristics are summarized in Table 1. A total of 134 lesions of 109 patients were detected and assessed. A total of 93 HCCs were detected in 79 patients (79/201, 39.3%). Of the 93 HCCs identified, 59 (63.4%) were 1–1.9 cm, 34 lesions (36.5%) were 2 cm or larger, and the average lesion size was 1.81 cm. Lesions other than HCCs ($n = 41$) were considered cirrhotic nodules such as regenerative nodules or dysplastic nodules ($n = 29$), hemangiomas ($n = 10$), nodular fibrosis ($n = 1$), and focal eosinophilic infiltration ($n = 1$).

The reference standard was considered positive for HCC if the results of a pathologic examination within 12 months of the index MRI examination were positive ($n = 20$). In the remaining patients ($n = 73$), the diagnosis of HCC was based on the radiological hallmarks of American Association for the Study of Liver Diseases or the Korean Liver Cancer Study Group-National Cancer Center Korea, namely the arterial enhancement and washout on the portal venous or transitional phases (3, 4, 21, 22). After independent review, two reviewers re-evaluated the MR findings of each HCC in consensus in terms of the presence of findings favoring HCC to clarify the incidence of these findings.

Five cirrhotic nodules were confirmed by pathologic diagnosis, and the other 24 cirrhotic nodules were finally categorized as benign, following multidisciplinary board consensus. The reference standard for cirrhotic nodules was based on comprehensive contrast-enhanced MRI reading by radiologists 1 and 2 in consensus and no interval change in clinical

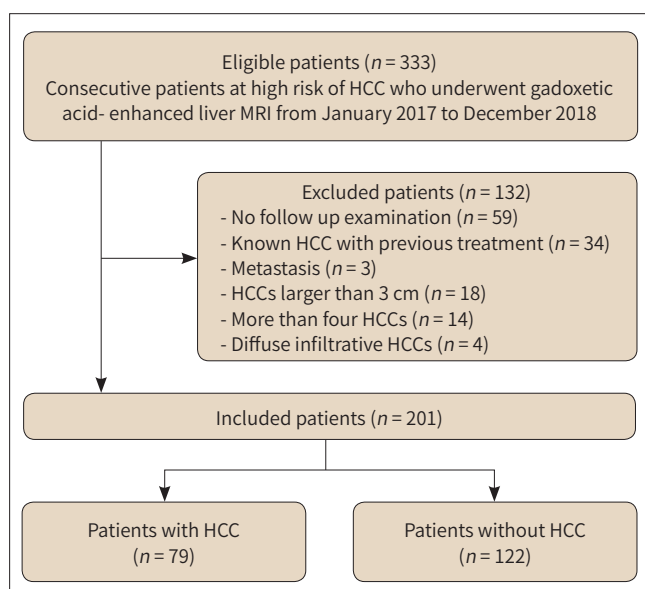


Fig. 1. Flow chart of the study population.
HCC = hepatocellular carcinoma

Table 1. Patients and Lesion Demographics

Characteristics	Patients with HCC (n = 79, 39.3%)	Patients without HCC (n = 122, 60.7%)	p-Value
Age (mean ± SD)	61.85 ± 9.95	57.57 ± 10.64	0.558
Sex, %			0.354
Male	18 (22.8)	35 (28.7)	
Female	61 (77.2)	87 (71.3)	
Etiology of liver disease, %			0.102
Hepatitis B	53 (67.1)	64 (52.5)	
Hepatitis C	3 (3.8)	9 (7.4)	
Alcoholic liver disease	16 (20.3)	40 (32.8)	
Others (NAFLD, AIH, etc.)	7 (8.8)	9 (7.4)	
Child Pugh score, %			0.816
A	62 (78.5)	97 (79.5)	
B	13 (16.4)	21 (17.2)	
C	4 (5.1)	4 (3.3)	
Lesion size (mm, number of lesions = 134)			0.010
10-19	59 (63.4)	29 (70.7)	
≥ 20	34 (36.6)	12 (29.3)	
Mean ± SD	1.90 ± 0.59	1.56 ± 0.49	

AIH = autoimmune hepatitis, HCC = hepatocellular carcinoma, NAFLD = non-alcoholic fatty liver disease, SD = standard deviation

and imaging follow-up examinations (at least a 12 months follow-up interval; mean interval, 18 months). Other lesions, such as hemangiomas, nodular fibrosis, and focal eosinophilic infiltration, were diagnosed based on characteristic imaging findings (23-25).

MRI TECHNIQUES

All images were obtained using a 3T MR scanner (MAGNETOM Tim Trio; Siemens Medical Solution, Erlangen, Germany) with a phased-array body coil. The CMRI protocols (Table 2) consisted of a breath-hold axial T1-weighted in- and out-of-phase two-dimensional volumetric interpolated breath-hold examination (VIBE) imaging. Breath-hold T2WI was acquired using fat-suppressed half-Fourier acquisition single-shot turbo-spin echo techniques, and heavily T2WI also underwent breath-hold half-Fourier-acquired single-shot turbo spin echo (HASTE) sequencing without fat suppression. For contrast-enhanced dynamic T1-weighted imaging using 3D VIBE, 0.1 mL/kg (0.25 mmol/mL) of GA (Primovist, Bayer Healthcare, Leverkusen, Germany) was injected with an MRI-compatible injector (Nemoto Kyorindo Co., Ltd., Tokyo, Japan) at a flow rate of 1 mL/sec, followed by a 20 mL 0.9% saline flush. The axial images were obtained at 30, 60, 120, 180, 600, and 900 s after injection of the contrast material, and 900 s (15 min) was considered for HBP imaging. Additionally, contrast-enhanced coronal images were obtained at 5 min. DWI with the simultaneous use of respiratory triggering was obtained in the axial plane by single-shot echo-planar imaging using three values ($b = 50, 400, \text{ and } 800 \text{ s/mm}^2$). An afferent diffusion coefficient (ADC) map was reconstructed on a pixel-by-pixel basis using the standard software on the console (Syngo, Siemens Healthineers, Erlangen, Germany).

Table 2. Imaging Parameters of the MRI Protocols

	In & Opposed Phase T1WI	T2WI & Heavily T2WI	Dynamic Contrast-Enhancement	DWI
Pulse sequence	VIBE	HASTE	VIBE	EPI
TR/TE (ms)	4.4/1.4 & 2.3	2000/81166	3.5/1.3	4500/76
Section thickness (mm)	3	5	3	5
Interslice gap (mm)	0	0.5	0	0.5
Flip angle (°)	9	90-150	13	
Field of view (mm)	300-400	300-400	300-400	300-400
Matrix number	320 × 256	320 × 256	352 × 194	160 × 120
B values (sec/mm ²)	-	-	-	50, 400, 800

DWI = diffusion-weighted imaging, EPI = echoplanar imaging, HASTE = half-Fourier-acquired single-shot turbo spin echo, TE = echo time, TR = repetition time, T1WI = T1-weighted imaging, T2WI = T2-weighted imaging, VIBE = volumetric interpolated breath-hold examination

The acquisition scan time for our full conventional liver MRI protocol, including dynamic phases after GA injection, was approximately 40 min, compared to approximately 10 min (including the setup) for the simulated AMRI protocol, which included T2WI (3-4 min), HBP imaging (1 min), and DWI (4 min).

IMAGE ANALYSIS

Two radiologists (both board-certified radiologists with 15 years and 5 years of experience, respectively, in abdominal imaging) who were blinded to the clinical information and pathologic analyses, independently assessed two sets of images (AMRI and CMRI) per patient. The two sets of AMRI and CMRI images were interpreted at different times, at least four weeks apart, to reduce recall bias.

In the simulated AMRI, for each patient, all lesions ≥ 10 mm were detected and their signal intensities on T2WI and HBP imaging were assessed. Radiologists measured the lesion size on the HBP image because overestimation of the lesion size could be made on T2WI and DWI (26). Lesions smaller than 10 mm were neglected. First, all lesions were scored according to the scoring system (Table 3) of a previous study (12). In the scoring system, very hyper-signal intensity on T2WI indicates bright signal intensity compared with signal intensity of the spleen, whereas very hypo-signal intensity on T2WI means absolutely dark signal intensity compared with the signal intensity of hepatic parenchyma. Then, the nodule categorization was adjusted according to the signal characteristics on DWI. The lesions with restricted diffusion showing high signal intensity on DWI and low signal intensity on the ADC map were upgraded by one category. The final score for each lesion was considered to be the highest final score for any nodule on that examination. Final imaging scores of 4 or 5 were interpreted as positive examinations.

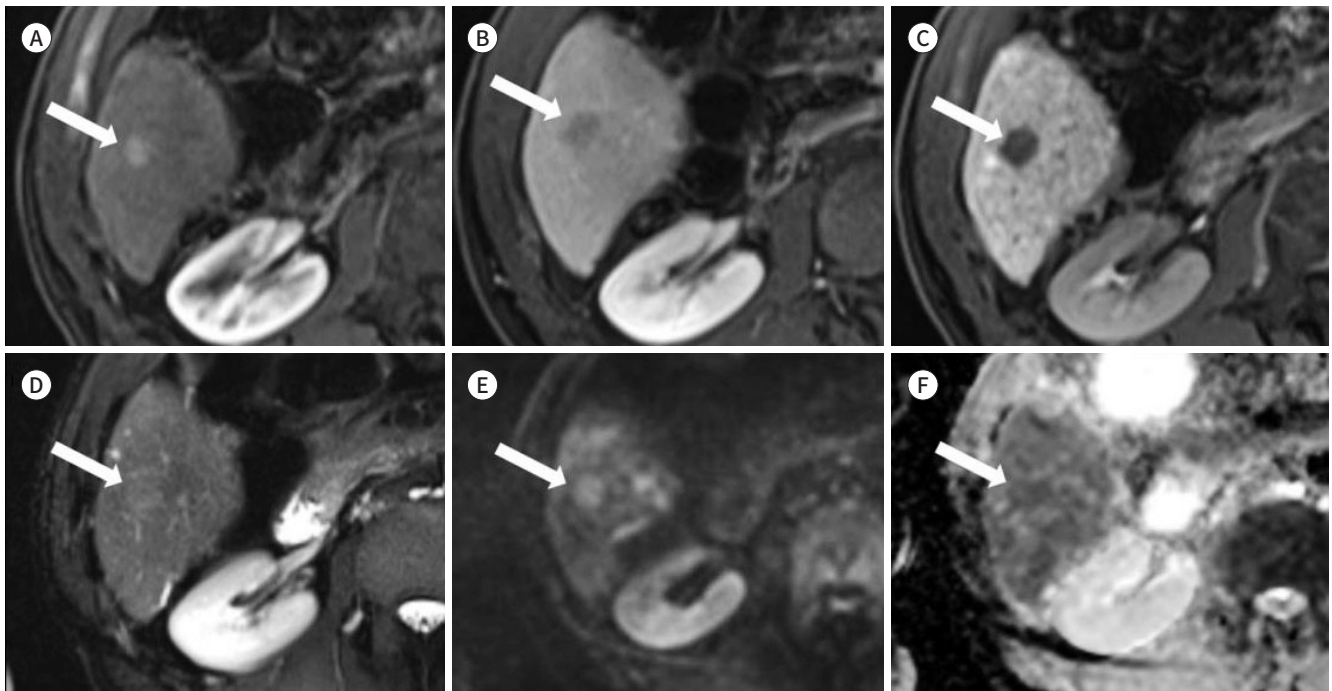
Separately, on the CMRI, all lesions ≥ 10 mm were detected and assessed according to LI-RADS v2018, using LI-RADS category 1 to 5 (27, 28). Lesions 10 mm or larger in the LI-RADS category of 4 and 5 were considered positive examinations (Fig. 2). Likewise, LI-RADS does not allow sub-centimeter observations to be considered definite HCC (27, 28). Sub-centimeter HCCs are unlikely to metastasize or become untreatable before the next surveillance ex-

Table 3. Scoring of Abbreviated MRI

	Hepatobiliary Phase Imaging		
	Hypointense	Isointense	Hyperintense
T2-weighted imaging			
Very hyperintense	2	2	2
Mildly hyperintense	5	4	4
Isointense	4	2	3
Mildly hypointense	4	3	3
Very hypointense	2	2	2

Fig. 2. A 52-year-old male with hepatocellular carcinoma.

A-F. The mass (arrows) shows arterial enhancement (**A**), washout on the portal phase (**B**), hypointensity on hepatobiliary phase imaging (**C**), subtle hyperintensity on T2-weighted imaging (**D**), and restricted diffusion on diffusion-weighted imaging (**E, F**). The final imaging score for abbreviated MRI and conventional MRI is 5 and interpreted as positive examinations.



amination six months to one year later.

STATISTICAL ANALYSIS

To analyze the inter-reader agreement between the two image sets, Cohen's k statistics were applied, where 0–0.20 indicated slight agreement, 0.21–0.40 indicated fair agreement, 0.41–0.60 indicated moderate agreement, 0.61–0.80 indicated substantial agreement, and 0.81–1.00 indicated almost perfect agreement (29). For each image set and reader, the per-patient sensitivity, specificity, PPV, negative predictive value (NPV), and accuracy were obtained with binominal 95% confidential intervals (CIs), to compare the per-patient diagnostic performance of the two AMRI and CMRI protocols.

All statistical analyses were performed using IBM SPSS Statistics for Windows, version 23.0 (IBM Corp., Armonk, NY, USA) and MedCalc software version 18.11.3 (MedCalc Software,

Mariakerke, Belgium). A *p*-value of less than 0.05 was considered significant.

RESULTS

INTER-READER AGREEMENT

Cohen's Kappa values for the two observers were 0.839 (0.764–0.915) for AMRI, and 0.948 (0.904–0.993) for CMRI, indicating that the inter-reader agreement between the two image sets was almost perfect for both image sets.

PER-PATIENT DIAGNOSTIC PERFORMANCE

In the AMRI, the mean per-patient sensitivity and NPV were 94.9% (95% CI: 90.3–97.8) and 96.4% (95% CI: 93.1–98.1), respectively. In the CMRI, the mean per-patient sensitivity and NPV were 96.2% (95% CI: 91.9–98.6) and 97.5% (95% CI: 94.6–98.8), respectively. A comparison of the mean sensitivity and NPV showed no statistically significant difference between the AMRI and CMRI (*p* > 0.05). Other per-patient diagnostic performance parameters for each set 1 and 2 are summarized in Table 4.

FALSE-NEGATIVE AND FALSE-POSITIVE LESIONS

There were six false-negative examinations on AMRI, two for both readers, two for reader A and two for reader B. Both readers scored the two AMRI examinations as score 1 or 2, whereas the CMRI showed single LI-RADS category 4 observations for each (probably HCC).

Reader A missed two mild hyperintense lesions on T2WI and isointense lesions on the HBP images of two patients, which were confirmed on follow-up dynamic enhanced CT and transarterial chemoembolization. Reader B missed one lesion with mild hypointensity on HBP imaging, but it was proven to be HCC in follow-up studies. Other lesions showing very hyperintensity on T2WI and hyperintensity on HBP were scored as score 2 by reader B on the

Table 4. Per-Patient Diagnostic Performance of AMRI and CMRI

	AMRI (%)	CMRI (%)	<i>p</i> -Value
Reader 1			
Sensitivity	94.9 (87.5–98.6)	98.7 (93.1–99.9)	0.060
Specificity	87.7 (80.5–93.0)	94.3 (88.5–97.7)	0.033
PPV	83.3 (75.6–89.0)	91.8 (84.4–95.8)	0.015
NPV	96.4 (91.1–98.6)	99.1 (94.3–99.9)	0.137
Accuracy	90.5 (85.6–94.2)	96.0 (92.3–98.3)	0.046
Reader 2			
Sensitivity	94.9 (87.5–98.6)	93.7 (85.8–97.9)	0.761
Specificity	86.1 (78.6–91.6)	95.1 (89.6–98.2)	0.004
PPV	81.5 (73.9–87.3)	92.5 (84.9–96.4)	0.002
NPV	96.3 (90.9–98.5)	95.9 (90.8–98.2)	0.960
Accuracy	89.5 (84.4–93.4)	94.5 (90.4–97.2)	0.096

Data are percentage (95% confidential interval).

AMRI = abbreviated MRI, CMRI = conventional MRI, NPV = negative predictive value, PPV = positive predictive value

AMRI due to hyperintensity on T2WI, but the CMRI showed a typical dynamic enhancement pattern of HCC with LI-RADS category 5, which was pathologically confirmed as HCC on surgery. There is no known malignancy other than HCC.

There were 22 false-positive examinations on AMRI, ten by both readers, five by reader A, and seven by reader B. Most of the false-positive lesions were presumed to be cirrhotic nodules (Fig. 3), such as regenerative nodules (RNs) and dysplastic nodules (DNs) (19/22, 86.4%). Other false-positive lesions were a hemangioma (1/22, 4.5%), nodular fibrosis (1/22, 4.5%), and focal eosinophilic infiltration (1/22, 4.5%). The cirrhotic nodules were hypointense lesions on HBP imaging (18/22, 81.8%), mild hyperintense lesions on T2WI (9/22, 40.9%), or restricted diffusion on DWI (4/22, 18.1%).

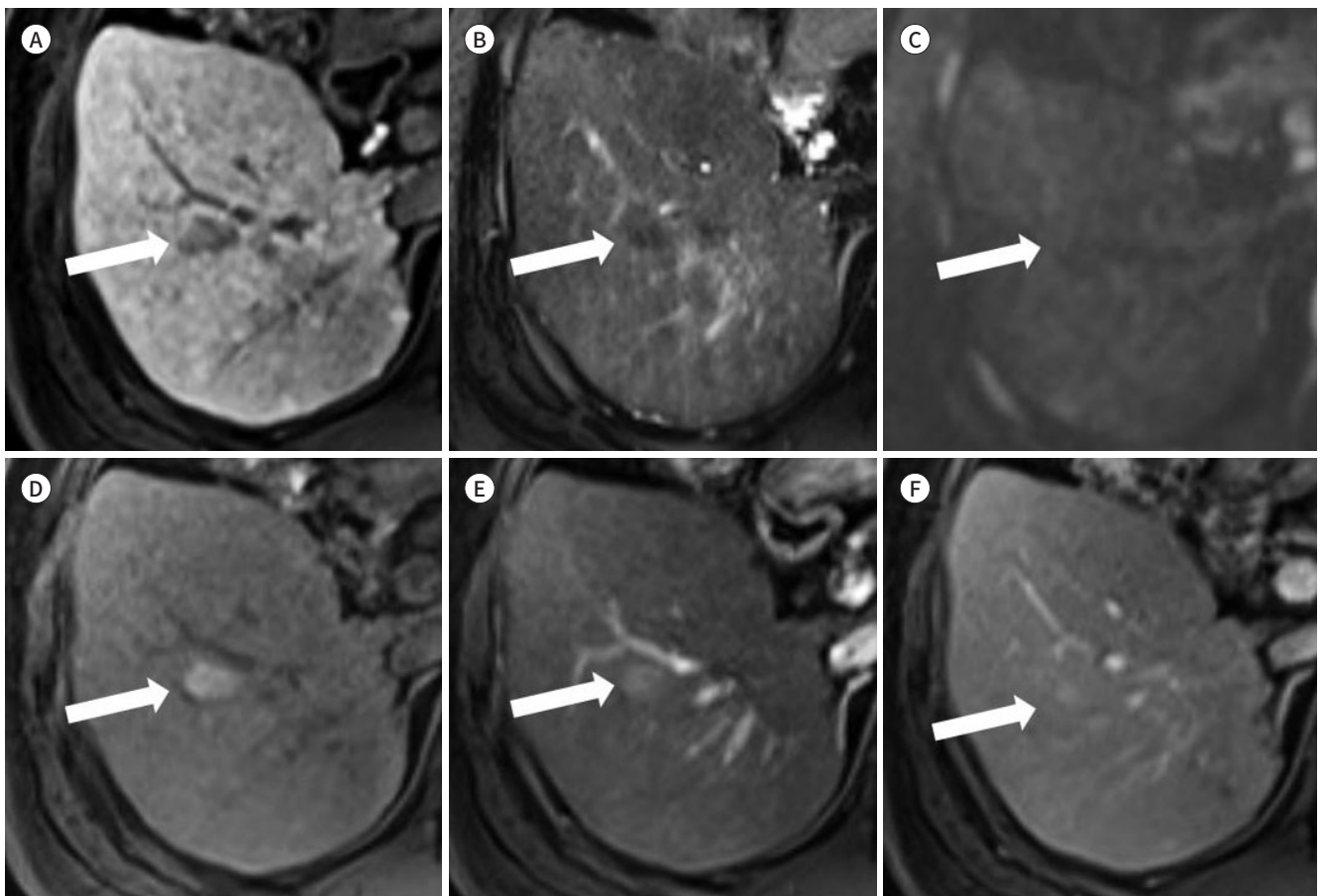
DISCUSSION

Our study simulated the performance of an AMRI by focusing on a subset of sequences,

Fig. 3. False positive lesion on AMRI in a 57-year-old male.

A-F. The nodule (arrows) showing hypointensity on hepatobiliary phase **(A)**, subtle hypointensity on T2-weighted imaging **(B)**, and no diffusion restriction on diffusion-weighted imaging **(C)** on AMRI, assigned a score of 4. However, on dynamic contrast-enhanced MRI, the nodule (arrows) showed hyperintensity on pre-contrast T1-weighted imaging **(D)**, no enhancement on arterial phase image **(E)**, and washout on portal phase image **(F)**. The tumor marker was within the normal range and the nodule was stable at the 18-month follow-up; it was considered a benign cirrhotic nodule.

AMRI = abbreviated MRI



including T2WI, HBP, and DWI. The advantage of AMRI is that it is a shortened version of the CMRI examination of the liver for the surveillance of HCC in cirrhotic patients. AMRI, including T2WI, HBP imaging, and DWI, can be performed at a lower cost in a shorter time than CMRI, thus making it more suitable for routine HCC screening (11-13, 16). The T2WI sequence of MRI serves to differentiate benign cysts and some hemangiomas from malignant lesions, such as HCC (30). Most lesions of non-hepatocyte origin, including HCC as well as benign lesions, show hypointensity on HBP imaging, which can explain the high sensitivity of MRI (31, 32). DWI is included to potentially detect HCC nodules that are not recognized or reported on other acquisitions (33, 34).

Our study showed that the inter-reader agreement was almost perfect, which means that this method might be generalizable. The mean per-patient sensitivity and NPV of AMRI were 94.9% and 96.4%, respectively. In contrast, the mean per-patient sensitivity and NPV of CMRI were 96.2% and 97.5%, respectively. The AMRI in our study had sensitivity and NPV in the surveillance of early stage HCC, clinically comparable to CMRI with full sequences. One report (15) showed that the sensitivity of each of the two readers was 88.0% and 86.2% in the detection of early HCC on unenhanced AMRI, which was lower than that of our results. This is because our study performed AMRI, including HBP imaging. Besa et al. (11) reported that AMRI including HBP imaging had a per-patient sensitivity of 80.6% and an NPV of 94.2%. Marks et al. (12) reported that the mean per-patient sensitivity and NPV were 82.6% and 93.2%, respectively. The NPVs in previous studies including HBP imaging (11, 12) were similar to our results, but the sensitivities were lower than in our study. Although previous studies included large-sized advanced HCCs, they showed lower sensitivity compared to our study. The reason why the sensitivity of our study was good compared to the previous study may be that our study used only 3T MRI with good resolution and thin slice thickness of the HBP imaging, whereas previous studies used 1.5T or thick slice thickness of the HBP imaging.

In our study, there were several false-negative cases where mild hyperintensity on T2WI or mild hypointense lesions on HBP imaging were not detected and missed, probably due to a background of heterogeneous hepatic parenchyma. Patients with cirrhotic liver, a known common risk factor for HCC, show a multinodular appearance of mixed-signal intensity or diffuse heterogeneous appearance, which obscures small lesions. This is a relatively common limitation in ultrasound, which is currently used for screening for HCC as well as AMRI (7, 35, 36).

The per-patient specificity of our study was relatively low due to the higher false-positive rate of AMRI. Most of the false-positive lesions were presumed to be cirrhotic nodules, following multidisciplinary board consensus. Typically, RNs show iso- to hypointensity on T2WI, iso- to hyperintensity on HBP imaging, and DN demonstrate variable signal intensity on T2WI and HBP images (37, 38). In clinical practice, if there are positive lesions suspected of HCC in screening AMRI protocols, dynamic contrast-enhanced MRI needs to be considered.

In our study, it took 30-40 min to perform the CMRI examinations. On the other hand, AMRI could be completed within 10 min if the GA injection was performed outside the MRI scanner. AMRI has a very short scan time because AMRI uses only a few sequences compared to CMRI, so it can be expected to be inexpensive and more beneficial to patients. A few studies have compared the cost effectiveness of AMRI for HCC surveillance (11, 39). Besa et

al. (11) found a 30%–35% cost saving when using a similar AMRI consisting of HBP imaging and DWI compared to a full contrast-enhanced CMRI. In a study to evaluate the cost-effectiveness of risk-stratified HCC screening, AMRI had a lower incremental cost-effectiveness ratio and was the most cost-effective strategy across a wide range of HCC incidences compared with ultrasound, CT, and CMRI (39). Further numerical verification is needed to accurately identify cost reductions.

Our study has several limitations. First because of the retrospective study design, there was a selection bias in patient sampling. The prevalence of HCC in this study is higher than that in a prospective study (9). We are concerned about the overestimation of the performance of AMRI. Further prospective research is needed to confirm our results. However, all examinations were performed within a single center and with a single 3T MRI, which may not necessarily translate to scanners of different model or field strength. Second, the benign lesions in this study included hemangiomas, cirrhotic nodules, and focal inflammatory or fibrotic lesions. Although these benign liver lesions are common and their differentiation from hypervascular HCCs is an important diagnostic issue, no other types of benign liver lesions were included. Finally, histopathologic confirmation of the lesions was not available, and consensus reading of the MRI and follow-up clinical studies were used as the reference standard based on guidelines for diagnosing HCC (3, 4, 20).

In conclusion, AMRI using only three sequences had a comparable sensitivity and NPV, compared to CMRI for the screening of early stage HCC in cirrhotic patients. Therefore, it could be an alternative HCC screening tool for high-risk HCC patients. A multi-center prospective trial is needed to confirm these findings.

Author Contributions

Conceptualization, L.E.S., J.Y.Y.; data curation, all authors; formal analysis, all authors; investigation, L.E.S., K.S.M., S.S.S.; methodology, L.E.S., S.S.S., J.Y.Y.; project administration, J.Y.Y.; resources, L.E.S., S.S.S., J.Y.Y.; software, all authors; supervision, J.Y.Y.; validation, all authors; visualization, L.E.S., J.Y.Y.; writing—original draft, L.E.S.; and writing—review & editing, J.Y.Y.

Conflicts of Interest

The authors have no potential conflicts of interest to disclose.

Funding

None

REFERENCES

1. Bray F, Ferlay J, Soerjomataram I, Siegel RL, Torre LA, Jemal A. Global cancer statistics 2018: GLOBOCAN estimates of incidence and mortality worldwide for 36 cancers in 185 countries. *CA Cancer J Clin* 2018; 68:394-424
2. Yuen MF, Lai CL. Screening for hepatocellular carcinoma: survival benefit and cost-effectiveness. *Ann Oncol* 2003;14:1463-1467
3. Marrero JA, Kulik LM, Sirlin CB, Zhu AX, Finn RS, Abecassis MM, et al. Diagnosis, staging, and management of hepatocellular carcinoma: 2018 practice guidance by the American Association for the Study of Liver Diseases. *Hepatology* 2018;68:723-750
4. European Association for the Study of the Liver. EASL clinical practice guidelines: management of hepatocellular carcinoma. *J Hepatol* 2018;69:182-236
5. Omata M, Cheng AL, Kokudo N, Kudo M, Lee JM, Jia J, et al. Asia-Pacific clinical practice guidelines on the

management of hepatocellular carcinoma: a 2017 update. *Hepatol Int* 2017;11:317-370

6. Singal A, Volk ML, Waljee A, Salgia R, Higgins P, Rogers MA, et al. Meta-analysis: surveillance with ultrasound for early-stage hepatocellular carcinoma in patients with cirrhosis. *Aliment Pharmacol Ther* 2009; 30:37-47
7. Tzartzeva K, Obi J, Rich NE, Parikh ND, Marrero JA, Yopp A, et al. Surveillance imaging and alpha fetoprotein for early detection of hepatocellular carcinoma in patients with cirrhosis: a meta-analysis. *Gastroenterology* 2018;154:1706-1718.e1
8. Hanna RF, Miloushev VZ, Tang A, Finklestone LA, Brejt SZ, Sandhu RS, et al. Comparative 13-year meta-analysis of the sensitivity and positive predictive value of ultrasound, CT, and MRI for detecting hepatocellular carcinoma. *Abdom Radiol (NY)* 2016;41:71-90
9. Kim SY, An J, Lim YS, Han S, Lee JY, Byun JH, et al. MRI with liver-specific contrast for surveillance of patients with cirrhosis at high risk of hepatocellular carcinoma. *JAMA Oncol* 2017;3:456-463
10. Cruite I, Schroeder M, Merkle EM, Sirlin CB. Gadoxetate disodium-enhanced MRI of the liver: part 2, protocol optimization and lesion appearance in the cirrhotic liver. *AJR Am J Roentgenol* 2010;195:29-41
11. Besa C, Lewis S, Pandharipande PV, Chhatwal J, Kamath A, Cooper N, et al. Hepatocellular carcinoma detection: diagnostic performance of a simulated abbreviated MRI protocol combining diffusion-weighted and T1-weighted imaging at the delayed phase post gadoxetic acid. *Abdom Radiol (NY)* 2017;42:179-190
12. Marks RM, Ryan A, Heba ER, Tang A, Wolfson TJ, Gamst AC, et al. Diagnostic per-patient accuracy of an abbreviated hepatobiliary phase gadoxetic acid-enhanced MRI for hepatocellular carcinoma surveillance. *AJR Am J Roentgenol* 2015;204:527-535
13. Lee JY, Huo EJ, Weinstein S, Santos C, Monto A, Corvera CU, et al. Evaluation of an abbreviated screening MRI protocol for patients at risk for hepatocellular carcinoma. *Abdom Radiol (NY)* 2018;43:1627-1633
14. Park SH, Kim B, Kim SY, Shim YS, Kim JH, Huh J, et al. Abbreviated MRI with optional multiphasic CT as an alternative to full-sequence MRI: LI-RADS validation in a HCC-screening cohort. *Eur Radiol* 2020;30:2302-2311
15. Han S, Choi JI, Park MY, Choi MH, Rha SE, Lee YJ. The diagnostic performance of liver MRI without intravenous contrast for detecting hepatocellular carcinoma: a case-controlled feasibility study. *Korean J Radiol* 2018;19:568-577
16. Tillman BG, Gorman JD, Hru JM, Lee MH, King MC, Sirlin CB, et al. Diagnostic per-lesion performance of a simulated gadoxetate disodium-enhanced abbreviated MRI protocol for hepatocellular carcinoma screening. *Clin Radiol* 2018;73:485-493
17. Chan MV, McDonald SJ, Ong YY, Mastrocostas K, Ho E, Huo YR, et al. HCC screening: assessment of an abbreviated non-contrast MRI protocol. *Eur Radiol Exp* 2019;3:49
18. Forner A, Reig ME, De Lope CR, Bruix J. Current strategy for staging and treatment: the BCLC update and future prospects. *Semin Liver Dis* 2010;30:61-74
19. Singal AG, Pillai A, Tiro J. Early detection, curative treatment, and survival rates for hepatocellular carcinoma surveillance in patients with cirrhosis: a meta-analysis. *PLoS Med* 2014;11:e1001624
20. Heimbach JK, Kulik LM, Finn RS, Sirlin CB, Abecassis MM, Roberts LR, et al. AASLD guidelines for the treatment of hepatocellular carcinoma. *Hepatology* 2018;67:358-380
21. Yoon JH, Park JW, Lee JM. Noninvasive diagnosis of hepatocellular carcinoma: elaboration on Korean Liver Cancer Study Group-National Cancer Center Korea practice guidelines compared with other guidelines and remaining issues. *Korean J Radiol* 2016;17:7-24
22. Korean Society of Abdominal Radiology. Diagnosis of hepatocellular carcinoma with gadoxetic acid-enhanced MRI: 2016 consensus recommendations of the Korean Society of Abdominal Radiology. *Korean J Radiol* 2017;18:427-443
23. Chan YL, Lee SF, Yu SC, Lai P, Ching AS. Hepatic malignant tumour versus cavernous haemangioma: differentiation on multiple breath-hold turbo spin-echo MRI sequences with different T2-weighting and T2-relaxation time measurements on a single slice multi-echo sequence. *Clin Radiol* 2002;57:250-257
24. Ohtomo K, Baron RL, Dodd GD 3rd, Federle MP, Ohtomo Y, Confer SR. Confluent hepatic fibrosis in advanced cirrhosis: evaluation with MR imaging. *Radiology* 1993;189:871-874
25. Kim YK, Kim CS, Moon WS, Cho BH, Lee SY, Lee JM. MRI findings of focal eosinophilic liver diseases. *AJR Am J Roentgenol* 2005;184:1541-1548
26. Seuss CR, Kim MJ, Triolo MJ, Hajdu CH, Rosenkrantz AB. Comparison of MRI pulse sequences for predic-

- tion of size of hepatocellular carcinoma at explant evaluation. *AJR Am J Roentgenol* 2014;203:300-305
27. Chernyak V, Fowler KJ, Kamaya A, Kielar AZ, Elsayes KM, Bashir MR, et al. Liver Imaging Reporting and Data System (LI-RADS) version 2018: imaging of hepatocellular carcinoma in at-risk patients. *Radiology* 2018; 289:816-830
 28. Stoller DW. *Magnetic resonance imaging in orthopaedics and sports medicine*. Philadelphia: Lippincott Williams & Wilkins 2007
 29. Landis JR, Koch GG. The measurement of observer agreement for categorical data. *Biometrics* 1977;33: 159-174
 30. Kim YK, Lee YH, Kim CS, Han YM. Added diagnostic value of T2-weighted MR imaging to gadolinium-enhanced three-dimensional dynamic MR imaging for the detection of small hepatocellular carcinomas. *Eur J Radiol* 2008;67:304-310
 31. Ahn SS, Kim MJ, Lim JS, Hong HS, Chung YE, Choi JY. Added value of gadoxetic acid-enhanced hepatobiliary phase MR imaging in the diagnosis of hepatocellular carcinoma. *Radiology* 2010;255:459-466
 32. Sano K, Ichikawa T, Motosugi U, Sou H, Muhi AM, Matsuda M, et al. Imaging study of early hepatocellular carcinoma: usefulness of gadoxetic acid-enhanced MR imaging. *Radiology* 2011;261:834-844
 33. Piana G, Trinquart L, Meskine N, Barrau V, Beers BV, Vilgrain V. New MR imaging criteria with a diffusion-weighted sequence for the diagnosis of hepatocellular carcinoma in chronic liver diseases. *J Hepatol* 2011; 55:126-132
 34. Vandecaveye V, De Keyzer F, Verslype C, Op de Beeck K, Komuta M, Topal B, et al. Diffusion-weighted MRI provides additional value to conventional dynamic contrast-enhanced MRI for detection of hepatocellular carcinoma. *Eur Radiol* 2009;19:2456-2466
 35. Wong LL, Reyes RJ, Kwee SA, Hernandez BY, Kalathil SC, Tsai NC. Pitfalls in surveillance for hepatocellular carcinoma: How successful is it in the real world? *Clin Mol Hepatol* 2017;23:239-248
 36. Colli A, Fraquelli M, Casazza G, Massironi S, Colucci A, Conte D, et al. Accuracy of ultrasonography, spiral CT, magnetic resonance, and alpha-fetoprotein in diagnosing hepatocellular carcinoma: a systematic review. *Am J Gastroenterol* 2006;101:513-523
 37. Hussain SM, Semelka RC, Mitchell DG. MR imaging of hepatocellular carcinoma. *Magn Reson Imaging Clin N Am* 2002;10:31-52
 38. Yoneda N, Matsui O, Kitao A, Kozaka K, Kobayashi S, Sasaki M, et al. Benign hepatocellular nodules: hepatobiliary phase of gadoxetic acid-enhanced MR imaging based on molecular background. *Radiographics* 2016;36:2010-2027
 39. Goossens N, Singal AG, King LY, Andersson KL, Fuchs BC, Besa C, et al. Cost-effectiveness of risk score-stratified hepatocellular carcinoma screening in patients with cirrhosis. *Clin Transl Gastroenterol* 2017;8:e101

초기 간암 선별 검사로서 단축 자기공명영상 검사의 진단능: 고식적 역동학적 자기공명영상검사와의 비교

임은솔¹ · 김성모¹ · 신상수¹ · 허숙희² · 이종은¹ · 정용연^{2*}

목적 고위험 환자에서 초기 간암 선별 검사로서 단축 자기공명영상 검사의 환자별 진단능을 기존의 고식적 간 자기공명영상검사와 비교하고자 한다.

대상과 방법 간암 고위험군에서 간 자기공명영상 검사를 시행 받은 총 201명의 환자에 대해 연구를 시행하였다. 단축 자기공명영상 검사 군의 프로토콜은 T2 강조영상, 담도기 T1 강조영상, 확산강조영상 등으로 구성되며, 두 명의 영상의학과 의사가 각각의 환자에 대해 후향적으로 단축 자기공명영상검사 군 및 고식적 자기공명영상검사 군, 두 군의 영상을 독립적으로 평가하였다. 두 연구자 간 일관성은 Cohen's kappa 값을 이용하여 비교하였다. 복합적인 참조표준을 이용하여 두 군에서 각각 진단능을 평가하여 비교하였다.

결과 79 명의 환자에서 총 93개의 간암이 발견되었다. 두 연구자 간 일관성은 두 군에서 모두 매우 양호하였다($\kappa = 0.839, 0.948$). 단축 자기공명영상검사 군에서 민감도 및 음성예측도는 각각 94.9% 및 96.4%였으며, 이는 고식적 자기공명영상검사 군과 큰 차이를 보이지 않았다 (96.2%, 97.5%).

결론 단축 자기공명영상검사는 고식적 자기공명영상검사에 비교하여 임상적으로 허용 가능한 민감도와 음성예측도를 갖는다. 따라서 간암 고위험군 환자에서 간암 선별검사로서 새로운 대안이 될 수 있을 것이다.

¹전남대학교병원 영상의학과,

²화순전남대학교병원 영상의학과